Paper
Int'l J. of Aeronautical & Space Sci. 16(1), 8–18 (2015)
DOI: http://dx.doi.org/10.5139/IJASS.2015.16.1.8

Numerical simulation of aerodynamic characteristics of a BWB UCAV configuration with transition models

Young-Hee Jo*
Department of Aeronautical System Engineering, Hanseo University, Seosan 356-706, Korea

Kyoungsik Chang and Dong-Jin Sheen*****
Department of Aeromechanical Engineering, Hanseo University, Seosan 356-706, Korea

Soo Hyung Park***
Department of Aerospace Information Engineering, Konkuk University, Seoul 143-701, Korea

Abstract

A numerical simulation for a nonslender BWB UCAV configuration with a rounded leading edge and span of 1.0 m was performed to analyze its aerodynamic characteristics. Numerical results were compared with experimental data obtained at a free stream velocity of 50 m/s and at angles of attack from -4 to 26°. The Reynolds number, based on the mean chord length, is 1.25×106. 3D multi-block hexahedral grids are used to guarantee good grid quality and to efficiently resolve the boundary layer. Menter's shear stress transport model and two transition models (γ-Re_θ model and γ model) were used to assess the effect of the laminar/turbulent transition on the flow characteristics. Aerodynamic coefficients, such as drag, lift, and the pitching moment, were compared with experimental data. Drag and lift coefficients of the UCAV were predicted well while the pitching moment coefficient was underpredicted at high angles of attack and influenced strongly by the selected turbulent models. After assessing the pressure distribution, skin friction lines and velocity field around UCAV configuration, it was found that the transition effect should be considered in the prediction of aerodynamic characteristics of vortical flow fields.

Key words: UCAV, Nonslender Delta Wing, γ-Re_θ Model, γ Model

1. Introduction

Unmanned combat air vehicle (UCAV) is an unmanned air vehicle that is armed to accomplish tactical missions. Generally, a long duration of flight capability is necessary for a reconnaissance mission in UAV, whereas low observable capabilities like stealth and high maneuverability are required to increase survival rates of the UCAV. Thus, the blended wing body (BWB) type has the advantages of a high ratio of lift to drag and decreased radar cross section through minimizing the discontinuity surface between the body and wings. Also the lambda wing configuration, with its cranked wing, is used to increase its stealth characteristics, for example, in the planforms of the SACCON in Germany and the UCAV series in the USA.

The aerodynamic characteristics in the upper part of the delta wing are the primary leading edge vortex, which is generated from the interaction between the separated shear layer at the leading edge and the free stream, the secondary leading edge vortex, which happens when the reattached flow is separated again by the adverse pressure gradient in the span-wise direction, the vortex lift, which is an additional lift by the local suction pressure near the leading edge, the development and breakdown of the vortex, and the nonlinear behavior of the pitching moment by the movement of the vortex [1].

* Graduate student
** Professor, Corresponding Author: kschang76@hotmail.com
*** Professor

Received: November 5, 2014 Revised : February 26, 2015 Accepted: March 2, 2015

http://ijass.org pISSN: 2093-274x eISSN: 2093-2480

The delta wing is divided into slender and nonslender types depending on the swept angle; generally, the nonslender type corresponds to the case of an angle less than 65° (β < 65°). As the swept angle decreases, the effect of the vortex lift and the maximum of its lift coefficient decrease and the stall happens earlier [2]. The difference between the slender and nonslender wings is that the primary vortex on the upper surface of the wing is reattached at less than the center of the body and the dual primary vortex is generated in the case of the nonslender type. Also, the vortex breakdown is observed as mush less abrupt in terms of increased buffeting.

Because the behavior of the vortex is sensitive to some parameters, such as the swept angle [3, 4], the geometry of the leading edge [5, 6], angles of attack, and the Reynolds number or Mach number, careful geometric design of the UCAV is required to meet the requirements.

In recent years, the BWB UCAV model has been a hot issue in unmanned air vehicle concepts and some representative models are the 1303 UCAV developed by the US AFRL in conjunction with Boeing and SACCON (Stability and Control Configuration) by NATO RTO AVT-161. There have been studies to understand the flow behavior around the low sweep delta wings through experiments [5, 7] and to provide validation data for evaluation of the major CFD codes [6, 8, 9, 10].

In particular, the low speed aerodynamics and the flow around the BWB configuration are still a challenging problem (inconclusive) for computational validation, because the transition effects should be considered in the turbulence models in CFD [11,12,13]. Arthur and Petterson [12] conducted a computational study considering the natural transition, which is calculated from the linear stability theory and the e^N criterion, of the low-speed flow over the 1303 configuration. Their results are compared with the data from the wind-tunnel tests to show better predictions in the turbulence model, considering transitional effects, than in the fully turbulent model [12]. Roy and Morgand [13] investigated the effects of the two transition modelings: the Habiballah-Delcourt criteria for the longitudinal transition and the Arnal-Coustols criterion for the crossflow instability mode around the SACCON [13] configuration. Their results show that the laminar-to-turbulent transition appears upstream of the wing as the incidence rises but comparisons with experimental results from infrared thermography became difficult.

There are three main methods to predict the transition locations around the aerodynamic body. The first one is 'classical,' the e^N method, based on linear stability theory to calculate the growth of the disturbance amplitude. The second approach is the low-Re turbulence model, which can only be applied to the bypass transition. The third one is to use the experimental correlation, while considering the free stream turbulence intensity and the local pressure gradient. Besides these methodologies, Menter et al. [14] proposed a new local correlation-based transitional model (LCTM), which solves two other transport equations, one for the intermittency (γ) and one for the transition onset criteria (Re_θ), based on the SST k-ω model. The LCTM approach has the advantage of predicting the transitional point from the transport equation with empirical correlations instead of the modeling of transition physics. This γ-Re_θ model shows good agreement with experimental data with transitional flows, such as the aerospatial A airfoil, the McDonald Douglas 30P-30N flap, and the DLR F 5 Wings [14]. Recently, Menter and Smirnov [15] simplified previous γ-Re_θ models to solve a single equation for the intermittency γ including the crossflow instability mechanism and model Re_θ locally by the free stream turbulence intensity and the pressure gradient in the correlation formula. This reduces the computational cost by solving one transport equation and avoids the dependency of Re_θ on the velocity U. The C1 correlation by Arnal was adopted to reflect the crossflow instability. This γ model shows a better prediction of the transition location at different Reynolds numbers and crossflow transition through the simulation of an infinite swept NLF(2)-415 wing.

In the present study, numerical simulations on the geometry of the BWB UCAV configuration were conducted and the aerodynamic coefficients are compared with the experimental results by Shim et al. [16]. In particular, the predictive capabilities of the model, considering the transition effects (γ-Re_θ model and γ model), were assessed based on comparisons with the results from the fully turbulent model. Also, the relationship between the pitching moment and vortex structures are investigated.

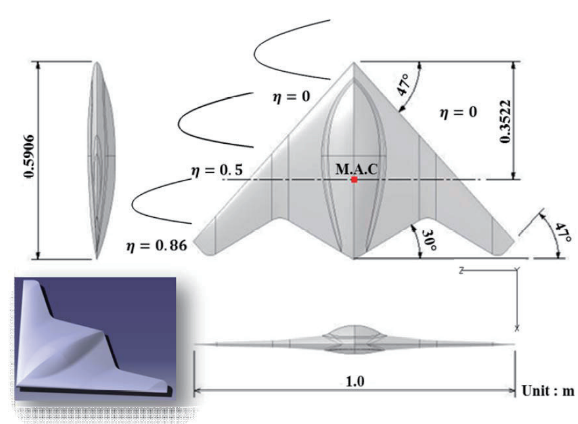

Fig. 1. Dimensions of a UCAV geometry

2. Numerical method and simulation set-up

Shim et al. [16] conducted wind tunnel tests on the geometry of the BWB configuration with a velocity of 40-60 m/s and a span of 1 m. In the present study, the same geometry is adopted, the specifications of which are shown in Fig. 1, with a swept angle of 47°, and the crank angle of 30° and a span of 1 m. The mean aerodynamic chord is 0.3522 m. The leading edge is round until η = 0.86 from the center of the model in the span-wise direction and the end of the wing and the trailing edge are sharp.

The length of the computational domain was 20C (C is the root chord length). The height and width of the computational domain are set to 15C. Because the angle of the side slip is not considered in the present study, a symmetric condition is applied to the surface of half geometry. (Fig. 2)

The grid and computational domain in the present study were generated with commercial software, ICEM-CFD of ANSYS [17]. A hexahedron structured cell was adopted to decrease the skewness of the grid system and to minimize the diffusion of the numerical errors. However, the sharp edge at the wing tip and the trailing edge make it difficult to use the topology of the O-type or C-type. Thus, the grid was generated in the H-type with multi-blocks (Fig. 2).

In the present work, three kinds of grid systems (coarse, medium, and fine mesh) were adopted for the grid test (Table 1). In the medium grid, 280 grid points are distributed in the stream-wise direction and clustered near the leading edge and the trailing edge with an interval of 1.4×10^{-4}C.

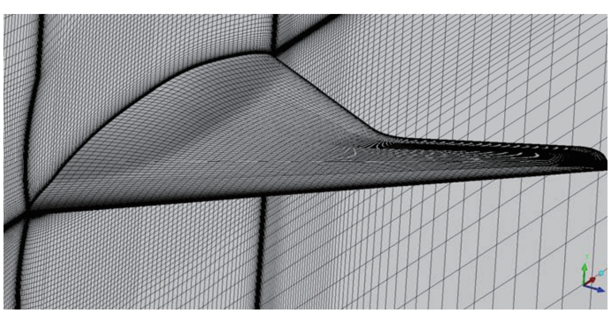

Fig. 2. Surface grids of UCAV

The numbers of grid points in the vertical and span-wise directions were 220 and 130, respectively. To resolve the boundary layer correctly, the first point is set to 2×10^{-5}C in all three grids, to confirm that y^+ is less than 1.0 over the surface after simulation. The fine grid has 1.5 times the grid points in a stream-wise direction and 1.8 times the points in a span-wise direction of the coarse grid and corresponds to the 0.5 wall unit in the vertical direction at a zero angle of attack.

The commercial CFD code, ANSYS Fluent 15.0, has been used to solve the incompressible Navier-Stokes equations. In the present work, the second-order discretization scheme in space and time was adopted and the correction of the pressure-velocity was done using a SIMPLEC algorithm. The time step is set to 0.002 s and the total simulation time is 2.6 s, corresponding to 1300 time steps and six times the total computational length ($216C_{root}$).

The free stream velocity is 50 m/s and the Reynolds number, based on the mean chord and the free stream velocity, is 1.25×10^{6}. To meet the experimental conditions of Shim et al. [16], atmospheric conditions at sea level were used. The boundary condition of the pressure outlet is applied to the far boundary and the wall of the UCAV is treated as a no-slip wall.

One fully turbulent model and two transitional models were used to simulate flow around the BWB type UCAV; Menter's shear stress transport (SST) model showed excellent results in previous research [10,12], the γ-Re_θ model, which considers the transitional effects of laminar-to-turbulent flows proposed by Menter and Langtry [14], and the γ model with crossflow effects [15].

For efficient simulation and fast convergence, a steady simulation with a 1st-order accuracy scheme was done and then an unsteady simulation with a 2nd-order scheme was performed. The criterion of convergence is that the residual of the continuity and turbulent quantities is less than 10^{-6}.

3. Results

The grid test was achieved using three grids based on the SST model (Table 1). Fig. 3 shows the lift coefficients versus

Table 1. Grid parameters of three grid systems

	Coarse	Medium	Fine
Streamwise direction	100	128	150
Vertical direction	80	110	110
Spanwise direction	92	130	166
Wing surface cells	1.8×10^4	3.9×10^4	5.2×10^4
Total cells	4.9×10^6	7.8×10^6	1.5×10^7

four angles of attack (0, 8, 16, and 24°) in three grids. The lift coefficients were predicted nearly consistently between medium and fine grids; however, those of the coarse grid show a maximum 6.2% difference versus those of the other two grids. Thus, the medium grid (cell number, 7.8×10^6) was selected as the appropriate one for efficient computation in the present study.

Figure 4 shows the aerodynamic coefficients with respect to the angles of attack of the three turbulence models (Menter's SST, γ-Re_θ model, γ model) and the experimental results by Shim et al. [16]. These coefficients are averaged out during 36 s (tU_{inf}/C_{root}) after the solution converged fully. In the experimental results [16], the lift curve is linear up to the angle of attack, 12°, and then the slope starts to decrease after 12°. Finally, the lift slope is flat after 20°, caused by the decrease in the vortex lift from the early breakdown of the leading edge vortex up to the apex [9]. The present results show good agreement with the experimental results [16] up to 12° and a small discrepancy after this angle, where the predictions of the γ-Re_θ model and γ model are slightly better than that of the Menter's SST model. This discrepancy can be explained from two points of view; one is that the present work does not consider the sting mounting, which is attached to the experimental model [11] and the other is the limitation that Reynolds-Averaged Navier-Stokes (RANS) models cannot capture the separated flow correctly at high angles of attack. In the plot of drag coefficient (Fig. 4(b)), two simulations show overall agreement with the reference data [16] except at an angle of attack less than 4°. The error between the three simulations and the experiment is the maximum at the angle of attack, 0°, where the experimental value is 0.00717. Menter's SST model overpredicted this as 0.01083 (+51%) and the γ-Re_θ model underpredicted it as 0.00579 (-19%). The best prediction was obtained through the γ model, which predicted 0.00732 (+2%). Because the γ-Re_θ model considers some regions of laminar flow and others in turbulent flow, the lower prediction of the drag than the fully turbulent model (Menter's SST model) seems reasonable. Also, these trends

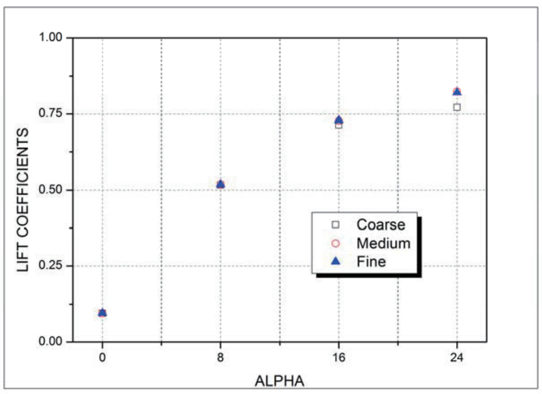

Fig. 3. Time averaged global lift coefficient of three grids

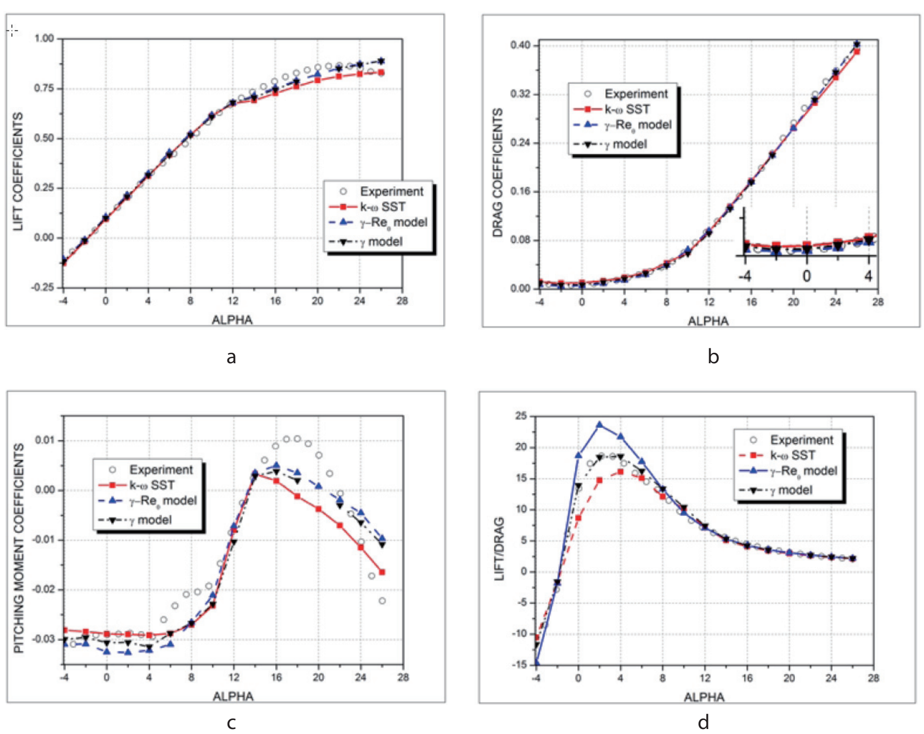

Fig. 4. Time averaged global aerodynamic coefficient against AoA(a : lift coefficient, b : drag coefficient, c : pitching moment coefficient, d : lift-to-drag ratio)

are observed in the comparison of airfoil simulations with fully turbulent model and transition models [14]. As the angle of attack increases, the plot shows that the prediction of two transition models is slightly better than that of the SST model. The pitching moment, as shown in Fig. 4(c), is predicted as a lower value at a low angle of attack and an overall trend, such as an increase of the pitching moment after the pitch break (~6°) and a decrease after the peak, agree well with experimental results. Nevertheless, all models fail to predict the change of the slope (between 6° and 10°) of the pitching moment. At low angles of attack, Menter's SST model predicts well, whereas all models show similar predictions where the slope is constant after the pitch break (10-14°). The angle of attack at the peak of the pitching moment is predicted as 16° and 14° in two transitional models and in the SST model separately, which is 2-4° smaller value than experimental one, 18°. The results show a discrepancy at a high angle of attack in numerical simulations, consistent with the tendency in lift coefficients. When the lift-to-drag ratio (L/D) is plotted in Fig. 4(d), the γ model shows the best prediction whereas the γ-Re_θ model overpredicts the peak of the lift-to-drag ratio and the Menter's SST model shows a contrary result.

Figure 5 shows the contours of the pressure coefficient and skin friction line (streamlines calculated from the wall shear stress) at a zero angle of attack. Top, middle, and bottom plots relate to Menter's SST model, the γ-Re_θ model, and the γ model, respectively. Indexes 'a' and 's' indicate the attachment line and separation one. In Menter's SST model, all flows are attached over the upper surface without separation, whereas in the two models there are laminar separations and reattachments of the separation bubbles, which correspond to the transition from laminar to turbulent, near 70% from the apex (x/C_{root} = 0.7). The difference between two transitional models is whether the separation region in the inboard is predicted. In experiments [16] of the same geometry with the similar flow conditions (Reynolds number based on the mean chord length is 8.5×10^5), the flow over the inboard wing is attached until the

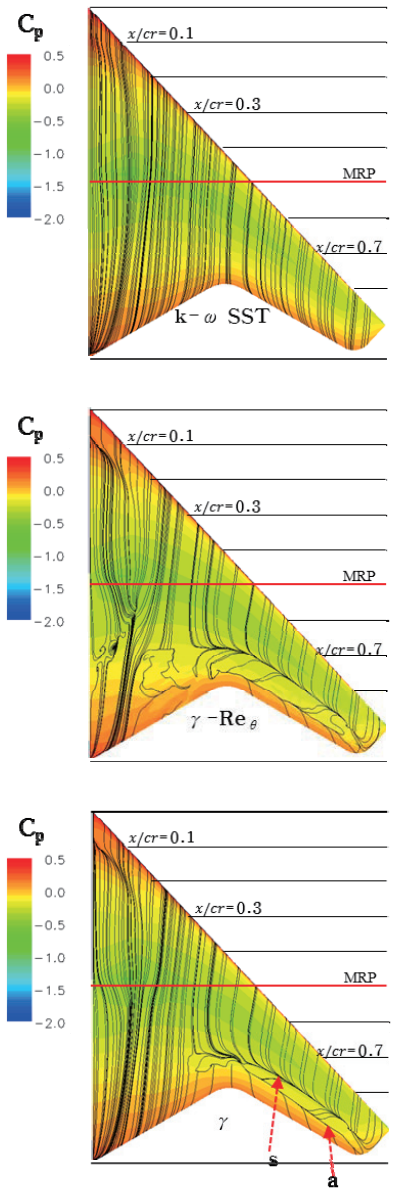

Fig. 5. Surface Cp contour and skin friction lines at α=0° (a : attachment, s : separation)(top : Menter SST model, middle : γ-Reθ model, bottom : γ model)

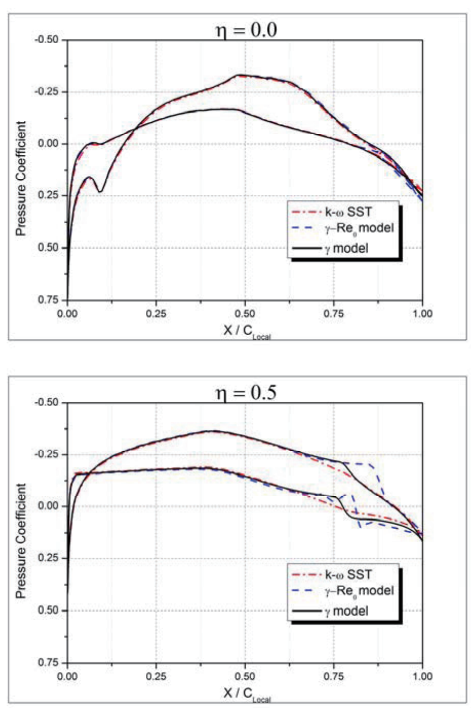

Fig. 6. Pressure coefficient Cp distribution at two spanwise locations η=0.0 and η=0.5

trailing edge of the wing at the angle of attack 8°, through oil flow visualization. Based on this result, the γ model shows a better prediction than the γ-Re_θ model. Also, when the more accurate prediction of the drag coefficient by the γ model is considered at an angle of attack of 0° (Fig. 4 (b)), the flow pattern of transitional models are more reasonable.

The pressure coefficient at two specified span-wise positions (one is the center line of $\eta = z/b = 0.0$ and the other is $\eta = z/b = 0.5$) is plotted in Fig. 6. The pressure distributions of all models are nearly consistent, except near the transitional points (x/C_{root}=0.75), where there are separation bubbles and reattachments. The fact that the pressure coefficient does not increase smoothly (smooth adverse pressure gradient) and remains constant to abrupt increases shows the typical behavior of separation and reattachment in the flow over an airfoil. [18]

The pressure contours and skin friction lines at the angle of attack, 14°, which is after the pitch break and shows approximately the same value of the pitching moments of all models, are shown in Fig. 7. In the results of γ-Re_θ model, the leading edge vortex starts to develop near the point of $x/C_{root} = 0.1$ and the separated flow can be seen over most regions, except the fuselage. However, Menter's SST model and the γ model predict that flow is attached mostly to the inner part of the wing and fuselage. The size of the suction pressure region near the leading edge is predicted to be the smallest in the Menter SST model. Although there is a definite difference in flow structures between models, the values of the pitching moment are nearly consistent. The reasons for these results are thought to be: 1) the regions with a large difference of suction pressure between models are near the point of the moment reference point (MRP = 0.3011 m from the apex), which causes a small effect in the momentum due to the shorter distance, and 2) the separation and vortex breakdown near the end of the wing, which has a great effect on the pitching moment, can be captured in all models.

Figure 8 shows the local turbulence intensity contours at the same planes (η = 0.0 and 0.5) as in Fig. 6. Local turbulent intensity (Tu) is defined as $100/U_{inf}(2k/3)^{1/2}$[17]. This value is used to estimate the transitional onset positions where turbulent intensity begins to have a non-zero value. The two transitional models show laminar flow in the front region and turbulent flow in the rest, whereas the Menter SST model predicted a fully turbulent flow from the leading edge. In the prediction of the γ-Re_θ model, the transition happens earlier on the upper part than that on the lower one. However, the γ model shows a contrary tendency and the consideration of the crossflow instability makes a prediction of a more rapid transition onset than the γ-Re_θ model. This is confirmed from

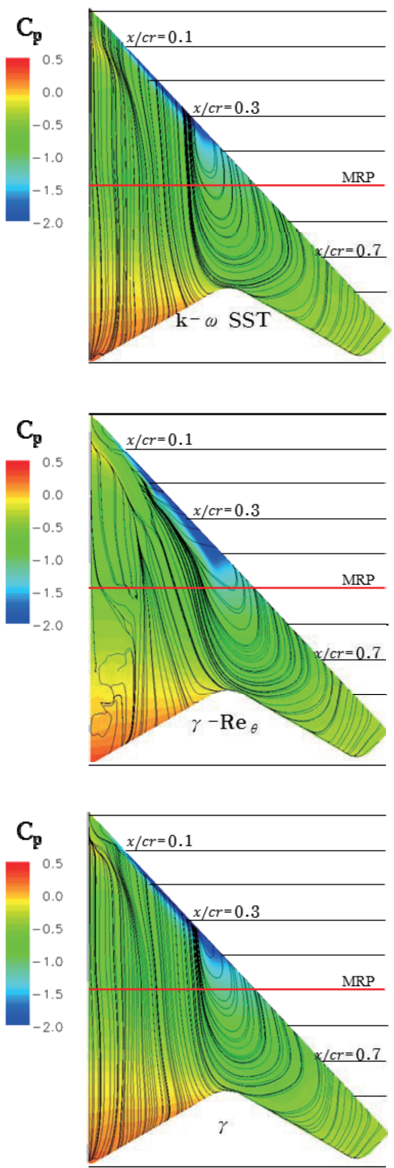

Fig. 7. Surface Cp contour and skin friction lines at α=14°

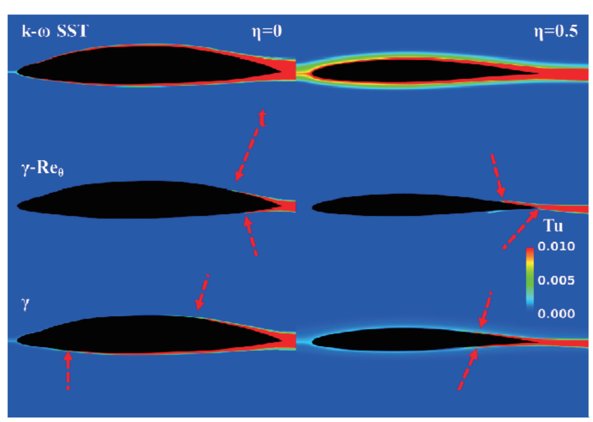

Fig. 8. Turbulent intensity contours on spanwise sectional planes

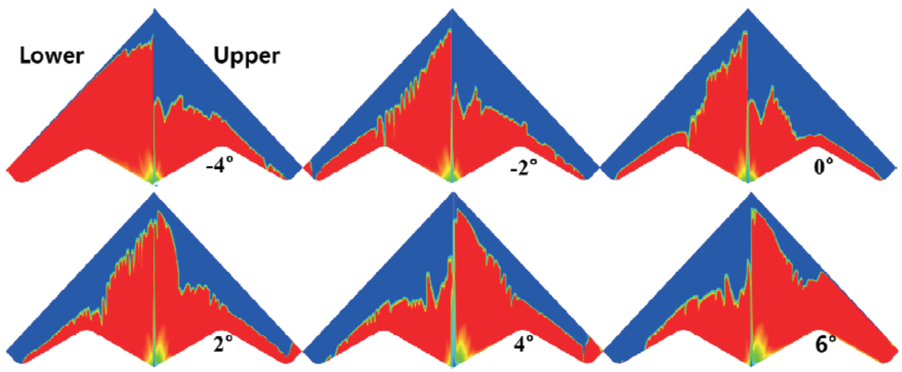

Fig. 9. Intermittency contours on lower and upper surface of γ model (Blue : laminar flow, Red : turbulent flow)

the distribution of the pressure coefficient in Fig. 6. For more accurate predictions of the transition onset position of the γ model, the contour of the intermittency (γ) at the upper part and the lower part of the body are plotted with respect to the six angles of attack (-4, -2, 0, 2, 4, 6°) in Fig.9. The value of γ means that the flow is laminar at γ = 0.0 and turbulent at γ = 1.0 [17]. As the angle of attack increases, the transition onset position at the pressure side goes backwards, whereas this position at the suction side moves forward. The variation of the transition points in the span wise direction is abrupt near the attached region between the wing and the convex geometry of the fuselage. The flow starts to be fully turbulent near the wing tip after an angle of attack of 2° and the fully turbulent region spreads to the inboard region of the wing with an increase in the angle of attack.

In this chapter, the vortical structures predicted by the three models will be investigated through vorticity contours and skin friction lines. Although there is a small discrepancy quantitatively between the numerical results and experimental ones, previous research [6] showed the qualitative similarity of the vortical structures between two methods. Fig. 10 shows the stream-wise vorticity (ω_x) contours with respect to each y-z plane in the cases with the angles of attack, 14°, 16° and 18°, where the pitching moment starts to nose down after the peak of the pitching moment. The leading edge vortex is separated into two primary vortexes and another vortex (the apex vortex) is generated from the apex at the inner part of wing. The apex vortex can be seen in the front of the MRP, which means this vortex induces a vortex lift to add to the pitching moment in the nose-up direction. This new apex vortex shares the attachment point with the leading edge vortex and then the attachment line is formed with a rapid decrease of the vorticity magnitude, confirming that the vortex breakdown was already ongoing. The skin friction lines over the upper surface show a flow separation pattern near the apex. As the angle of attack increases, vortex break down begins to occur, the magnitude of the vortex decreases, and the primary vortex in the inner part moves to the center (Fig. 10). The merger between the primary vortex and the apex vortex can be seen at an angle of attack of 18° in Fig. 10. At an angle of attack of 18°, two regions of laminar separation and suction pressure overlap and then two vortexes at the apex and leading edge start to merge. This phenomenon with the two primary vortexes and apex one shows that it can be captured clearly by two transitional models, but the strength of the vortex predicted by the Menter SST model was weak. Although laminar separation induces the development of the skin friction line from the apex, the vortex near the apex cannot be recognized clearly in Fig. 10. The reason is that the round shape, which delays the separation of the shear layer and depends more on the adverse pressure gradient by the thickness, makes it difficult to capture this vortex than the sharp one [9].

Figure 11 shows the contours of pressure coefficients and skin friction lines at angles of attack of 6°, 12°, and 18° to recognize the structure and position of the vortex of the three models. At an angle of attack of 6°, where the pitching moment starts to increase in the nose- up direction, wing tip separation occurs at x/C_{root} = 0.8 and suction pressures are forming from x/C_{root} = 0.4. The location of the separation is aft of the moment center and this causes the onset of lift loss and the nose-up pitching moment. However, there are still attached flows near the leading edge of the inboard wing. As the angle of attack increases, the region of separation increases, which is to be formed in most parts of the outboard wing, and the leading edge vortex moves forward with an increase in magnitude. This confirmed that the leading edge vortex starts to be formed at a distance from the apex and moves forward in the aerodynamics of the delta wing with a blunt leading edge. Finally, most upper surfaces have a separation flow region of 18°. From

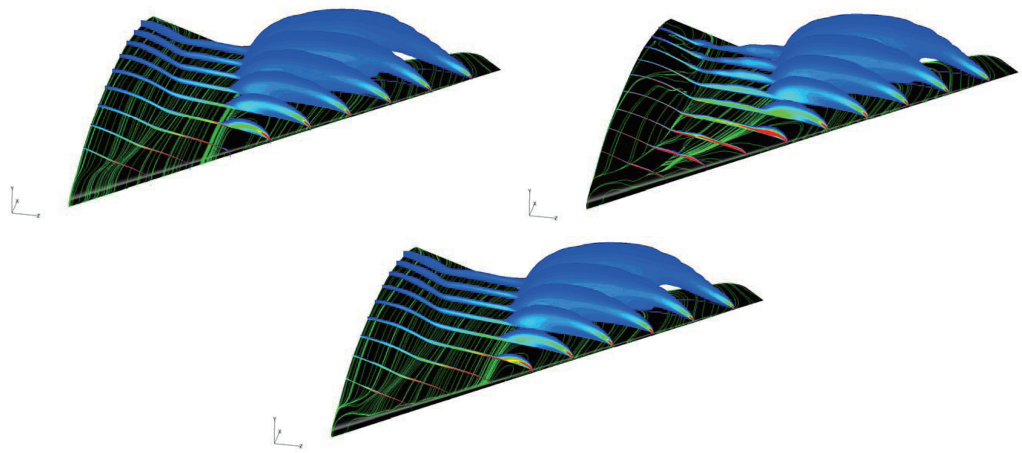

Fig. 10 (a). Axial vorticity and skin friction lines at α=14°(Left : Menter SST model, right : γ-Reθ model, bottom : γ model)

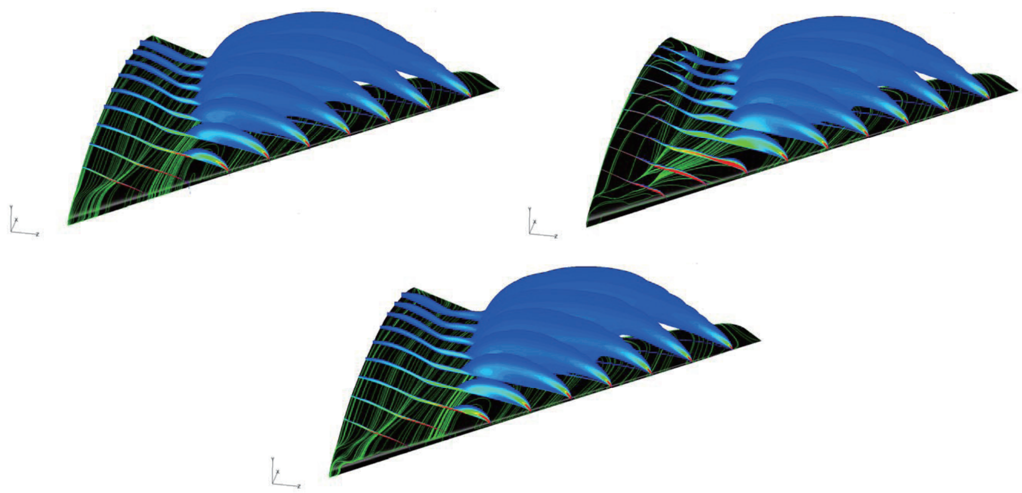

Fig. 10 (b). Axial vorticity and skin friction lines at α=16°(Left : Menter SST model, right : γ-Reθ model, bottom : γ model)

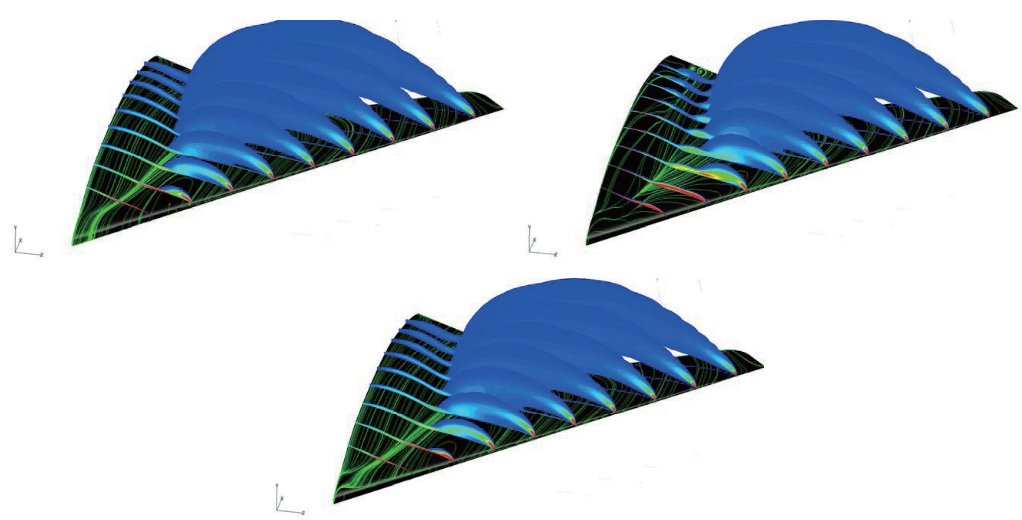

Fig. 10 (c). Axial vorticity and skin friction lines at α=18°(Left : Menter SST model, right : γ-Reθ model, bottom : γ model)

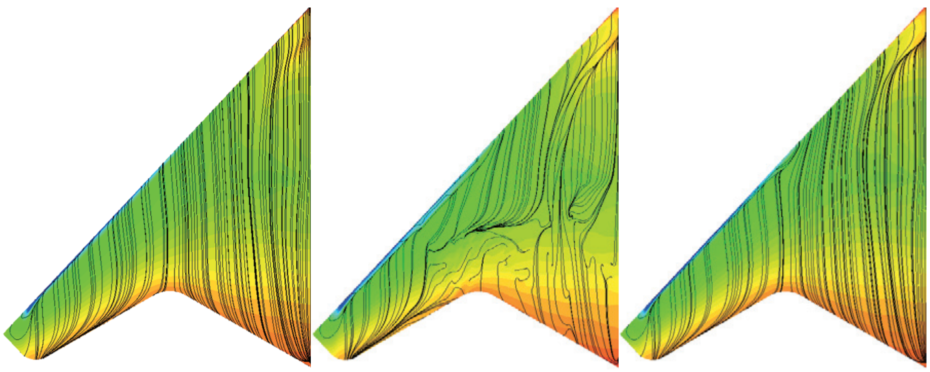

Fig. 11(a). Surface Cp contour and skin friction lines at α=6°(Left : Menter SST model, middle : γ-Reθ model, right : γ model)

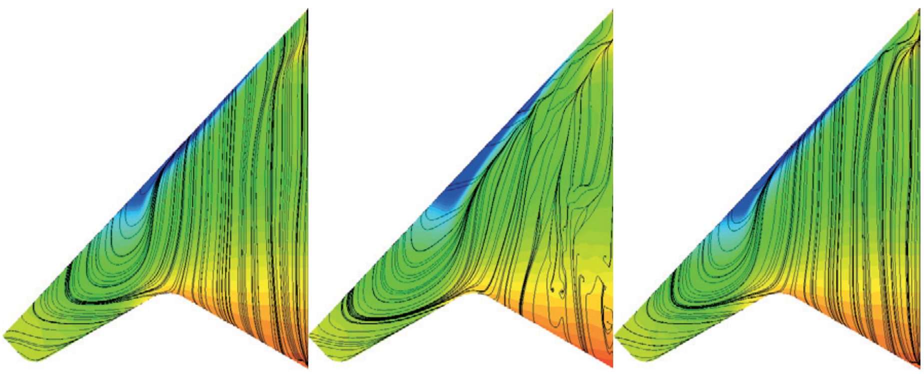

Fig. 11(b). Surface Cp contour and skin friction lines at α=12°

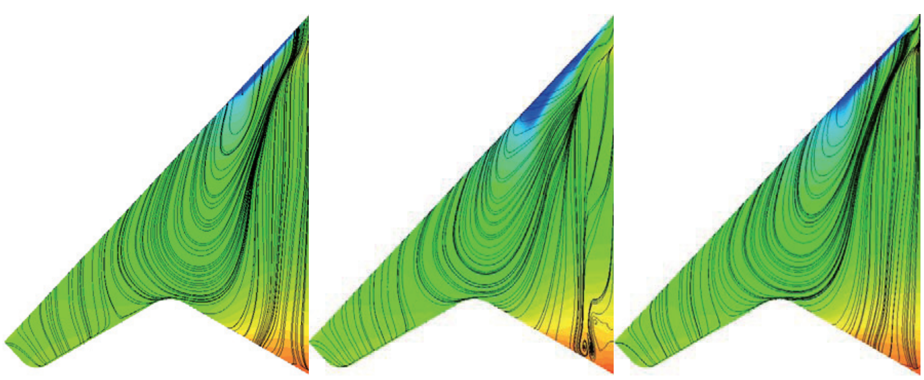

Fig. 11 (c). Surface Cp contour and skin friction lines at α=18°

the separation lines point of view, similar patterns are seen between the SST model and the γ model. However, the formations of suction pressures are similar between the γ-Re_θ model and the γ model.

Also, the reverse flow at the wing tip can be seen in the skin friction line, which can be confirmed from the contour of the axial velocity at the point of x/C_{root} = 0.8 in Fig. 12. The axial velocity has a negative value near the wing tip at an angle of attack of 8° and the generated vortex by this separation starts to break down and its magnitude decreases from an angle of attack of 8°, the 'critical angle of attack' [9]. All three models predict reverse flows at the angle of attack of 8°.

4. Conclusions

The present study reports results of simulations of the nonslender BWB UCAV configuration with one fully turbulent

DOI: http://dx.doi.org/10.5139/IJASS.2015.16.1.8

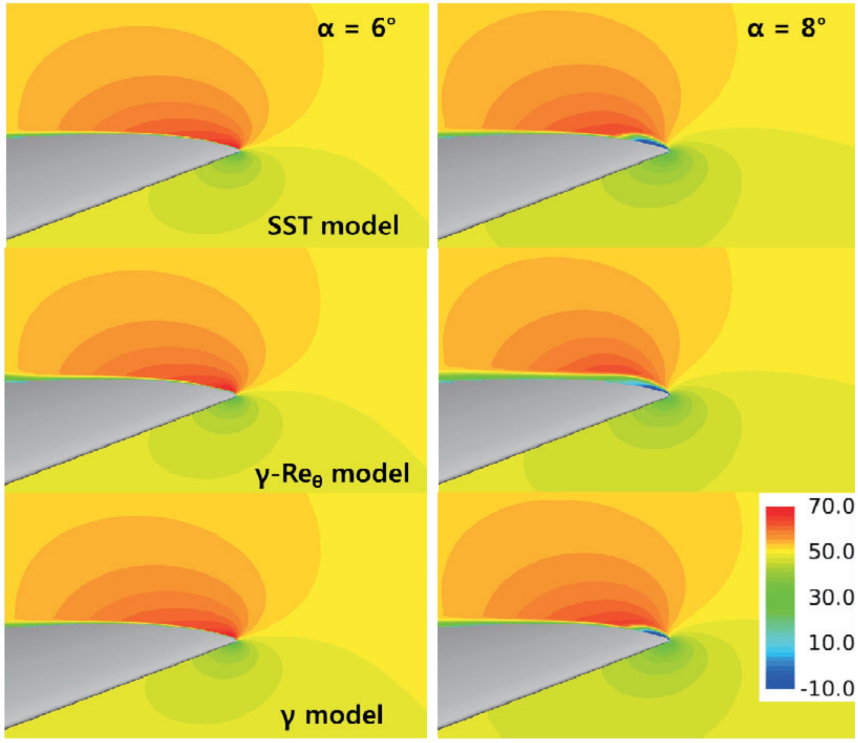

Fig. 12. Axial velocity contours at x/c=0.8

model (Menter SST model) and two transition models (the γ-Re_θ and γ models). The predictive capabilities of the two transition models were assessed from comparisons of aerodynamic coefficients, pressure contours, skin friction lines, and the vortical structures with experimental results [16].

In the comparisons of aerodynamic coefficients, the two transitional models were better than the fully turbulent model before and after the peak of the pitching moment. In the plot of lift-to-drag ratio, the prediction of the γ model, considering crossflow instability, was the best at low angles of attack. This confirmed the crossflow instability by the pressure gradient toward the span in the swept wing plays a more important role in enhancing the transition than Tollmien-Schlichting instability [19].

The findings through the contours of pressure coefficient and skin friction line were 1) that at a zero angle of attack, a fully turbulent model predicts all flows are attached without separation; however, the two transitional models show separation and re-attachment phenomena near the transition onset locations, and 2) as the angle of attack increased, separated flow was predicted near the leading edge in the case of the γ-Re_θ model, while the flow in the region of the inner part of the wing and fuselage was attached in the other models.

In the analysis of the vortex breakdown and merging between the primary vortex and the apex vortex, the prediction by the fully turbulent model was too weak to capture this phenomenon clearly, whereas the γ model predicted this well, even though the stream-wise vorticity is smaller than that of the γ-Re_θ model. Also, the prediction of the transition location in not only the upper surface, but also the lower one, is important in predicting the aerodynamic coefficients.

In conclusion, the transition models should be considered to simulate the low-speed flow around the BWB UCAV configuration. In future studies, we will investigate aerodynamic coefficients and flow structures numerically when the control surfaces and the attached engine are considered in a BWB configuration.

Acknowledgements

We acknowledge financial support from the Ministry of Science, ICT & Future Planning, subject to the project EDISON (EDucation-research Integration through Simulation On the Net, NRF-2011-0020560).

References

[1] John D. Anderson, JR, *Fundamentals of aerodynamics*, Fifth edition, McGraw-Hill.

[2] Earnshaw P. B. and Lawfird J. A., *Low-speed wind-tunnel experiments on a series of sharp-edge delta wings*, ARC Reports and Memoranda, No. 3424, 1964

[3] Gursul, I., Gordnier, R. and Visbal, M., "Unsteady aerodynamics of nonslender delta wings," Progress in Aerospace Science, Vol. 41, 2005, pp. 515-557.

[4] Jmanes M. Luckring, Okko J. Boelens, "A unit-problem investigation of blunt leading-edge separation motivated by AVT-161 SACCON research," NASA Technical Report, 2011

[5] Stephan C. Mcparlin, Robin J. Bruce, Anthony G. Hepworth and Andrew J. Rae, "Low speed wind tunnel on the 1303 UCAV concept," *24th AIAA Applied Aerodynamics Conference*, AIAA 2006-2985, 2006.

[6] Andreas Schutte, Dietrich Hummel and Stephan M. Hitzel, "Numerical and experimental analyses of the vortical flow around the SACCON configuration," *28th AIAA Applied Aerodynamics Conference*, AIAA 2010-4690, 2010.d

[7] Thomas D. Loeser, Dan D. Vicroy, and Andreas Schutte, "SACCON static wind tunnel tests at DNW-NWB," 28th AIAA Applied Aerodynamics Conference, AIAA 2010-4393, 2010.

[8] Milne, M. E., and Arthur M. T., "Evaluation of bespoke and commercial CFD methods for UCAV configuration," *24th Applied Aerodynamics Conference*, AIAA 2006-2988, 2006.

[9] Vallespin D., Ronch A. Da, Badcock K.J., and Boelens O., "Vortical flow prediction validation for an unmanned combat air vehicle model," Journal of Aircraft, Vol. 48, No. 6, 2011, pp. 1948-1959.

[10] Chi David, Chakravarthy Sukumar, and Goldberg Uri, "Flow prediction around the SACCON configuration using CFD++," *28th AIAA Applied Aerodynamics Conference*, AIAA 2010-4563, 2010.

[11] Petterson Kristian, "Low-speed aerodynamic and flowfield characteristics of a UCAV," *24th AIAA Applied Aerodynamics Conference*, 2006-2986.

[12] Arthur M.T., and Petterson K., "A computational study of the low speed flow over the 1303 configuration," *25th AIAA Applied Aerodynamics Conference*, 2007-4568, 2007.

[13] Le Roy, J. F., and Morgand S., "SACCON CFD static and dynamic derivatives using elsA," *28th AIAA Applied Aerodynamics Conference*, AIAA 2010-4562, 2010.

[14] Menter F.R., Langtry R. B., Likkl S. R., Suzen Y. B., Huang P. G.. and Volker S., "A correlation based transition model using local variables Part 1 – model formulation," ASME-GT2004-53452, 2004.

[15] Menter F. R. and Smirnov P., "Laminar-turbulent transition modeling based on a new intermittency model formulation," *11th World Congress on Computational Mechanics*, 2014.

[16] Shim H. J., Park S. O. and Oh S. Y., "An experimental study on aerodynamic coefficients of a tailless BWB UCAV," *KSAS Spring Conference*, 2013, pp. 110~113

[17] ANSYS FLUENT User's Guide.

[18] Shan H., Jiang L. and Liu C., "Direct numerical simulation of flow separation around a NACA 0012 airfoil," *Computers & Fluids*, Vol. 34, 2005, pp. 1096-1114.

[19] Shivaji M., *Correlation-based transition modeling for external aerodynamic flows*, Ph. D. diss., University of Maryland College Park, 2014.